INSTITUT DE FRANCE
Académie des sciences

Comptes Rendus

Physique

Zhesheng Chen, Jonathan Caillaux, Jiuxiang Zhang, Evangelos Papalazarou, Jingwei Dong, Jean-Pascal Rueff, Amina Taleb-Ibrahimi, Luca Perfetti and Marino Marsi

Ultrafast dynamics with time-resolved ARPES: photoexcited electrons in monochalcogenide semiconductors

Volume 22, Special Issue S2 (2021), p. 103-110

Published online: 3 May 2021
Issue date: 3 December 2021

https://doi.org/10.5802/crphys.57

Part of Special Issue: Physics of ultra-fast phenomena
Guest editors: Éric Collet (Université Rennes 1, CNRS, France) and Sylvain Ravy (Université Paris-Saclay, CNRS, France)

Les Comptes Rendus. Physique *sont membres du Centre Mersenne pour l'édition scientifique ouverte*
www.centre-mersenne.org
e-ISSN : 1878-1535

Comptes Rendus
Physique
2021, 22, nº S2, p. 103-110
https://doi.org/10.5802/crphys.57

Physics of ultra-fast phenomena / *Physique des phénomènes ultra-rapides*

Ultrafast dynamics with time-resolved ARPES: photoexcited electrons in monochalcogenide semiconductors

Zhesheng Chen [a, b, c], Jonathan Caillaux [a], Jiuxiang Zhang [a], Evangelos Papalazarou [a], Jingwei Dong [b], Jean-Pascal Rueff [c], Amina Taleb-Ibrahimi [c], Luca Perfetti [b] and Marino Marsi [*, a]

[a] Université Paris-Saclay, CNRS, Laboratoire de Physique des Solides, 91405 Orsay, France

[b] Laboratoire des Solides Irradiés, Ecole Polytechnique, CNRS, CEA, 91128 Palaiseau, France

[c] Synchrotron SOLEIL, L'Orme des Merisiers, Saint-Aubin, BP48, 91192 Gif-sur-Yvette, France

E-mails: zhesheng.chen@universite-paris-saclay.fr (Z. Chen), jonathan.caillaux@universite-paris-saclay.fr (J. Caillaux), jiuxiang.zhang@universite-paris-saclay.fr (J. Zhang), evangelos.papalazarou@universite-paris-saclay.fr (E. Papalazarou), jingwei.dong@polytechnique.edu (J. Dong), jean-pascal.rueff@synchrotron-soleil.fr (J.-P. Rueff), amina.taleb@synchrotron-soleil.fr (A. Taleb-Ibrahimi), luca.perfetti@polytechnique.edu (L. Perfetti), marino.marsi@universite-paris-saclay.fr (M. Marsi)

Abstract. Time-resolved ARPES makes it possible to directly visualize the band dispersion of photoexcited solids, as well as to study its time evolution on the femtosecond time scale. In this article, we show how this technique can be used to monitor the ultrafast hot carrier dynamics and the conduction band dispersion in two typical monochalcogenide semiconductors: direct band gap, *n*-type indium selenide and indirect band gap, *p*-type germanium selenide. With this approach, one can directly estimate the effective electron masses of these semiconductors. Moreover, the dynamics of hot electrons in the two semiconductors are analyzed and compared. Our findings provide valuable information for the use of monochalcogenide semiconductors in future optoelectronic devices.

Keywords. Time-resolved ARPES, Monochalcogenide semiconductor, Ultrafast dynamics, Effective mass, Out-of-equilibrium 2D materials.

Available online 3rd May 2021

* Corresponding author.

1. Introduction

The electronic structure is a unique characteristic of a crystalline solid and encodes crucial information that determines the material's electrical, magnetic and optical properties. Therefore, the efforts to understand the electronic structure in a solid have been one of the central themes of condensed matter physics, and angle resolved photoemission spectroscopy (ARPES) is one of the most direct experimental techniques to measure the energy band dispersion $E = E(\mathbf{k})$ [1]. From the functional point of view, not only the equilibrium electronic structure, but also its out-of-equilibrium properties play a crucial role in the response of the system to an external excitation. Time-Resolved ARPES, where photoemission spectroscopy is performed in a pump–probe configuration using ultrafast light pulses, makes it possible to extend to the excited states all the advantages of this method, providing the time evolution of the non-equilibrium system, $E = E(\mathbf{k}, t)$. Figure 1 shows a schematic diagram of the way time-resolved ARPES is implemented on the FemtoARPES setup [2].

In a semiconductor, the band gap is the main parameter determining device performance, and the dispersion of the conduction band (or valence band) is related to the electron (or hole) effective mass and consequently to the carrier mobility in a device [3–6]. For example, in indirect band gap semiconductors, the radiation recombination is far slower compared to direct band gap, as the absorption or emission of phonons need to be involved in the process, which is not suitable for light emission devices [7, 8]. In anisotropic semiconductors such as black phosphorus, the dispersions of conductions band along each high symmetric directions are significantly different, which corresponds to giant electron effective mass differences, and the mobility is highly direction dependent [9, 10].

ARPES is the most direct way to observe the electronic structure of a semiconductor with high energy and momentum resolution. For example, the electronic structure of indium selenide (InSe) has been directly observed by ARPES in a previous study, and it shows out-of-plane dispersions by changing photon energy, which indicates a quasi-two dimensional nature of the bulk material; in addition, if the electronic structure of InSe is modified with surface alkali atoms doping, the observed ∼1.3 eV band gap in bulk InSe is subsequently reduced as function of doping [11].

As mentioned above, time-resolved ARPES gives us the possibility to finely observe photoexcited empty electronic states as well as their ultrafast dynamics [12,13]. This approach has already been successfully applied to topological insulators, strongly correlated materials, and some semiconductors [14–18]. For example, in gallium arsenide (GaAs) Kanasaki *et al.* directly determined the energy-, momentum-, and time-resolved distribution of hot electrons photoinjected into the conduction band by time-resolved ARPES, and found an intervalley transition time as short as 20 fs [19]. In addition, by using the same method, we transiently occupied the conduction band of black phosphorus by an ultrafast pump pulse and measured the gap value with a subsequent probe pulse. The negligible band gap renormalization and Stark broadening have been observed and explained [10].

Van der Waals stacked monochalcogenide semiconductors such as indium selenide (InSe) and germanium selenide (GeSe) have attracted a lot of interest in recent years because of the widely tunable band gap as function of thickness and ultrahigh carrier mobility in field effect transistors (FETs). The carrier mobility in few-layer InSe is as high as 10^3 $\mathrm{cm^2 \cdot V^{-1} \cdot s^{-1}}$ and 10^4 $\mathrm{cm^2 \cdot V^{-1} \cdot s^{-1}}$ at room and low temperature, respectively [4, 7, 20–22]. This value is compatible to that found in graphene and is among the highest in 2D semiconductors. Compared to InSe, layered GeSe has a unique in-plane anisotropic crystal structure, and its optical properties also show an extremely anisotropic behavior, which open up possibilities for optoelectronic applications such as polarization-sensitive photodetectors and optical waveplates [23–26]. In this

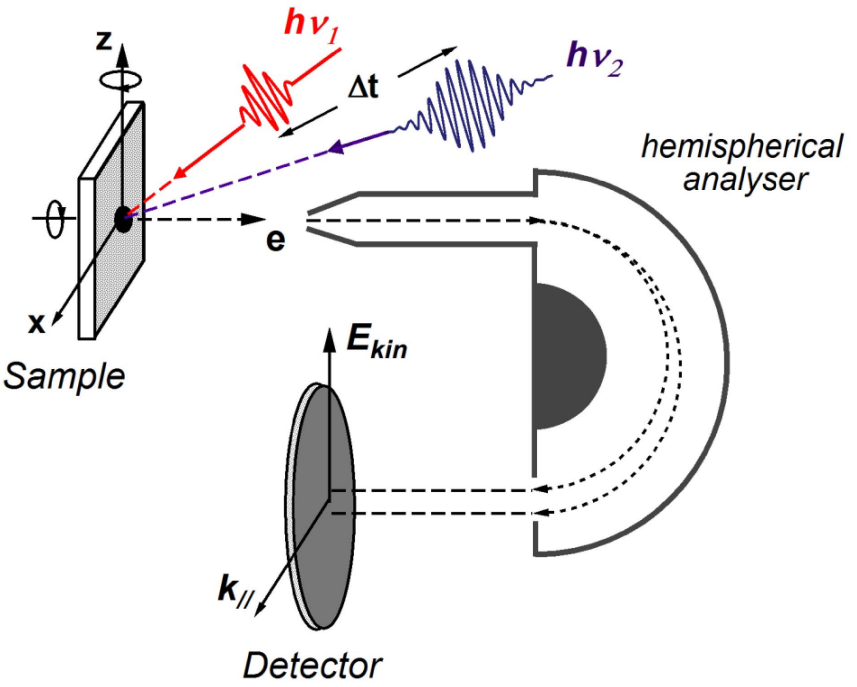

Figure 1. Schematic diagram of a time-resolved ARPES setup.

article we show how time-resolved ARPES can be used to investigate the photoexcited states in n-type InSe and p-type GeSe, and directly observe the dispersion of their conduction band and the hot carrier dynamics. The effective mass of the conduction band and hot carrier decay time are also extracted and compared. The study of the photoexcited states presented in this work provides important information for further applications of InSe and GeSe in novel optical and optoelectronic devices.

2. Experimental details

All the experiments have been performed on the FemtoARPES setup, using a Ti:sapphire laser system delivering 6 μJ pulses with a 250 kHz repetition rate [2]. Part of the laser beam (50 fs pulse, 1.57 eV) is used to pump the sample while the rest is employed to generate the 6.3 eV photons as probe pulse through cascade frequency mixing in BaB_2O_4 (BBO) crystals. The overall energy resolution of the experiment is ≅30 meV and the cross correlation between pump and probe pulses has full width at half maximum (FWHM) of 150 fs. High-quality single crystals of InSe (doped with Sn, 0.01%) we used have been grown using the Bridgmann method from a nonstoichiometric melt [11]. High-quality single crystal of GeSe was purchased from company of HQ graphene. The samples were cleaved and kept at the base pressure of 8×10^{-11} mbar. Our samples have been oriented by low energy electron diffraction and measured at the temperature of 135 K.

3. Results and discussion

The crystal structures of layered InSe and GeSe we used in this work are shown in Figure 2(a). InSe belongs to ε polytype and has hexagonal structure. The unit cell contains two parallel layers

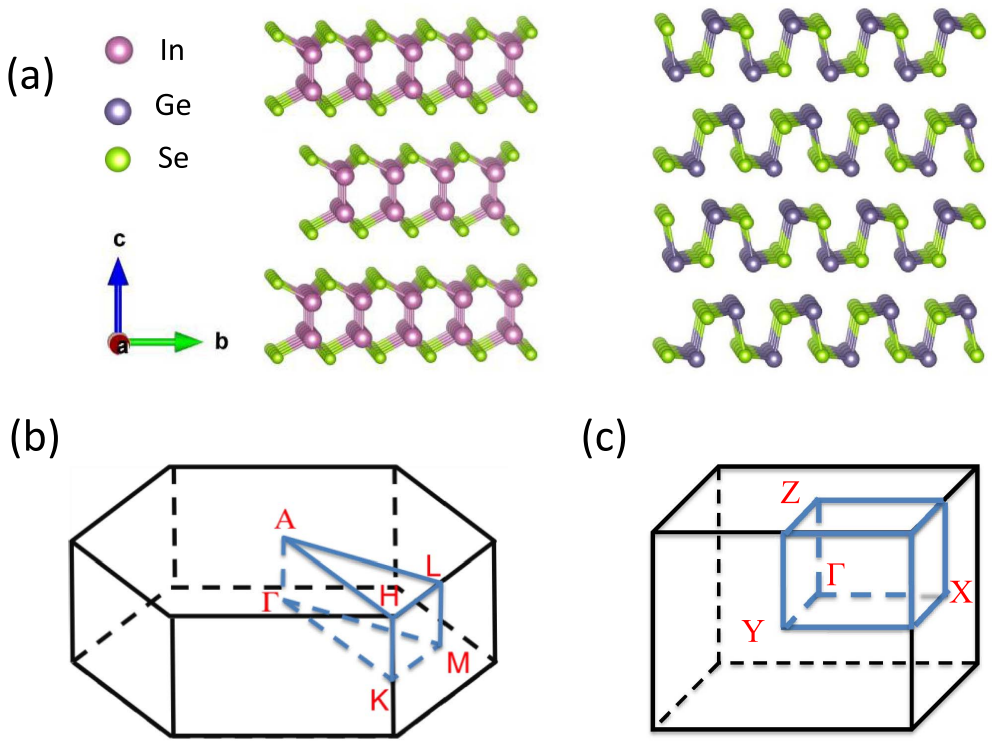

Figure 2. (a) Crystal structure of layered monochalcogenide semiconductors. Left: InSe. Right: GeSe. (b) Schematic of 3D Brillouin zone of InSe. (c) Schematic of 3D Brillouin zone of GeSe.

obtained by a translation of one layer onto another [27]. GeSe has a puckered structure similar to black phosphorus, and presents an orthorhombic crystal structure [28]. The schematics of the 3D Brillouin zones of InSe and GeSe are shown in Figure 2(b,c). Bulk InSe has a direct band gap of ~1.3 eV, with both conduction band minimum (CBM) and valence band maximum (VBM) centered in reciprocal (k) space, at the Γ point of the Brillouin zone [11, 29]. The Fermi level is inside the gap even though the sample is largely n-doped, as shown in the experimental data of Figure 3(a). After being pumped by the infrared-laser (1.57 eV), electrons in the valence band (occupied states) can be only photoexcited into the Γ valley of the conduction band (unoccupied states); other valleys cannot be reached as the maximum excess energy (E_{ex}) of electrons is ~0.27 eV (E_{ex} = 1.57 eV–1.3 eV) and the minimum energy difference between the adjacent valleys is ~0.7 eV (Γ valley to M valley). After a delay time, the photoexcited electrons are photoemitted by the ultraviolet laser probe (6.3 eV) from the conduction band to vacuum: the electron kinetic energy and momentum in k space can be thus determined by the electron energy analyzer (Figure 1). This makes it possible to observe the dispersion of the conduction band at time delay $t = 0$ and the dynamics of photoexcited electrons as a function of time delay.

Figure 3(a–d) shows the photoelectron intensity maps of InSe acquired along $\overline{\Gamma} - \overline{K}$ at different time delays between pump and probe. At negative delay of 1 ps, the system is in equilibrium conditions, and we don't observe electrons in CBM as the surface chemical potential is located below VBM, as shown in Figure 3(a). The position of the surface chemical potential depends on the doping level of the sample and also on band bending which can be slightly different for each cleaved surface. After photoexcitation, the excited electrons are transiently subject to the

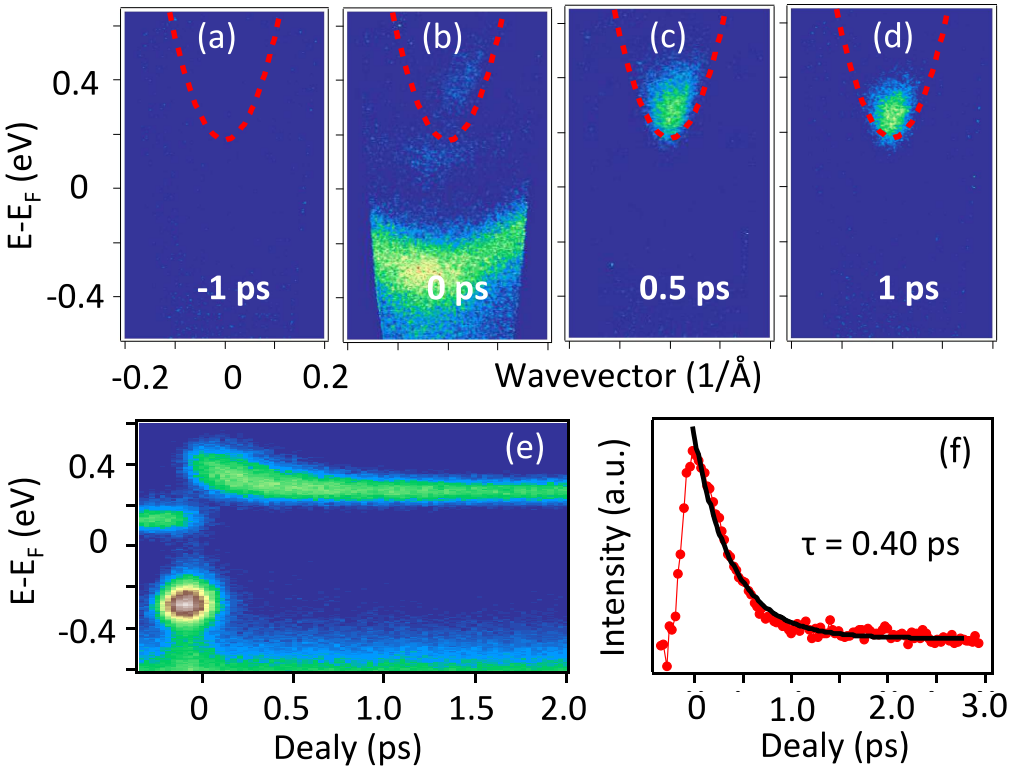

Figure 3. (a–d) Photoelectron intensity maps in InSe acquired along the $\overline{\Gamma}-\overline{K}$ direction and plotted for different delay times. The conduction band is fitted by a parabolic function and indicated by a red dashed line. (e) Dynamics of photoelectron intensity integrated in the wavevector interval $[-0.15, 0.15]$ Å^{-1}. (f) Intensity of electrons in the conduction band as a function of pump–probe delay. The black solid line is an exponential fit with decay time $\tau = 0.40$ ps.

attractive Coulomb potential from the holes as well as to the semiconductor polarization, which gives rise to two image potential states that are shown below the CBM. Image potential states are well understood on polarizable surfaces such as on bare metal surfaces, metal layers on metals, rare gas adlayers on different metallic substrates, and organic thin films on metal surfaces. To our knowledge, this is the first time that the image potential states are found on the surface of inorganic semiconductors. Moreover, we observe photoexcited electrons in the conduction band with the maximum excess energy of ~0.25 eV, as we estimated before. Such hot carrier cooling is a complex process that involves carrier–carrier, carrier–phonon, and phonon–phonon interactions. The dominant cooling process in InSe is carrier–phonon interaction, and generally there are two coupling mechanisms that drive electron–phonon scattering in inorganic semiconductors. The first one is polar Fröhlich interactions due to electron–LO phonon scattering for polar materials, that result from Coulomb interactions between the electrons and the macroscopic electric field induced by the out-of-phase displacements of oppositely charged atoms caused by the LO phonon mode. The second one is the electron-acoustic phonon scattering that is efficient at very low temperature. In InSe, the polar Fröhlich interactions via LO phonon emission is the dominant relaxation for hot carriers, allowing hot electrons to dissipate the energy in $\overline{\Gamma}$ valley and eventually cool down to CBM. In order to gain quantitative insight on the evolution of the

photoexcited states, we fit the dispersion of the $\overline{\Gamma}$ valley along $\overline{\Gamma}-\overline{K}$ by the parabolic expression $E = E_0 \pm p^2/2m_c$, where m_c is the effective mass for the conduction band. As shown by the dotted lines in Figure 3(b–d), the fitting curves reproduce with high accuracy the band dispersion with $m_c = 0.1 \pm 0.01 m_e$, where m_e is the free electron mass. The m_c of InSe extracted from the dispersion of the conduction band along $\overline{\Gamma}-\overline{K}$ in InSe is consistent in the values from other measurements such as transport and optical spectroscopy [20, 30]. Figure 3(e) shows the photoelectron intensity $I\,(E,\,t)$ integrated in the wavevector window $[-0.15, 0.15]$ Å^{-1} and plotted as a function of pump–probe delay. The total intensity of photoelectrons in the conduction band follows an exponential decay with time constant $\tau = 0.40 \pm 0.1$ ps, as shown in Figure 3(f). This timescale elucidates the main relaxation mechanism of hot carriers in the $\overline{\Gamma}$ valley, which is very similar to pristine InSe without Sn doping [29]. Therefore, we ascribe the short-time cooling process to the polar optical coupling with small momentum transfer.

Totally different from *n*-type bulk InSe with a direct band gap, pristine bulk GeSe is a *p*-doped semiconductor and has an indirect band gap. The CBM of GeSe locates at the center of Brillouin zone shown in Figure 2(c) and the gap is ~1.35 eV, which enables us to directly measure conduction band dispersion and hot carrier dynamics by time-resolved ARPES. From the photoelectron intensity maps along the zigzag direction ($\Gamma - Y$) shown in Figure 4(a–d), we observe the dispersion of photoexcited electrons in the conduction band at zero delay and positive delay. The chemical potential is ~0.7 eV below CBM, which confirms the *p*-type nature of the sample considering the indirect band gap of ~1.13 eV. Like for most semiconductors, we don't observe any image potential states, which can be explained by the different surface properties with respect to InSe. The maximum excess energy of hot electrons pumped by the infrared pulse is ~0.2 eV, which is similar to what found in InSe. However, the conduction band displays much less dispersion and one can fit it by the same parabolic function with $m_c = 1.8 \pm 0.1 m_e$. It is worth noticing that the m_c in GeSe is one order of magnitude larger than that of InSe, which might be the reason of significant mobility difference between the two materials. The photoelectron intensity $I\,(E,\,t)$ integrated in the wavevector window $[-0.2, 0.2]$ Å^{-1} and the total photoelectron intensity in the conduction band as a function of pump–probe delay are shown in Figures 4(e) and 4(f), respectively. The time constant of the hot carrier decay process is $\tau = 1.58 \pm 0.1$ ps by fitting the experimental data with exponential function, which indicates a much slower cooling process than that of InSe. Considering the similar maximum excess energy of photoexcited electrons in the conduction band of both materials, the time constant difference can be explained by the difference in energy or the phonons participating in the electron–phonon coupling process. On the other hand, the electron effective mass in GeSe is much larger than in InSe, and consequently the hot electron distribution in *k* space is very different. The distribution of hot electrons in InSe is within ± 0.1 Å^{-1} in *k* space, while their range is significantly lager (± 0.2 Å^{-1}) for GeSe. All of this can contribute to the difference between the hot carrier cooling processes in a direct band gap semiconductor like InSe and an indirect band gap semiconductor like GeSe. Further theoretical investigations will be necessary in order to clarify this issue.

4. Conclusions

In conclusion, we performed time-resolved ARPES on two different monochalcogenide semiconductors: direct band gap InSe and indirect band gap GeSe. The dispersion of the conduction band around the center of Brillouin zone and the corresponding hot electron dynamics are directly observed. The electron effective mass is extracted from the parabolic dispersion and the time constant of the decay process is obtained by exponential fittings. The electron effective mass in GeSe is much larger than that of InSe, and this is consistent with the significant large mobility in InSe found in previous studies. However, the decay process is much slower in GeSe, which might be

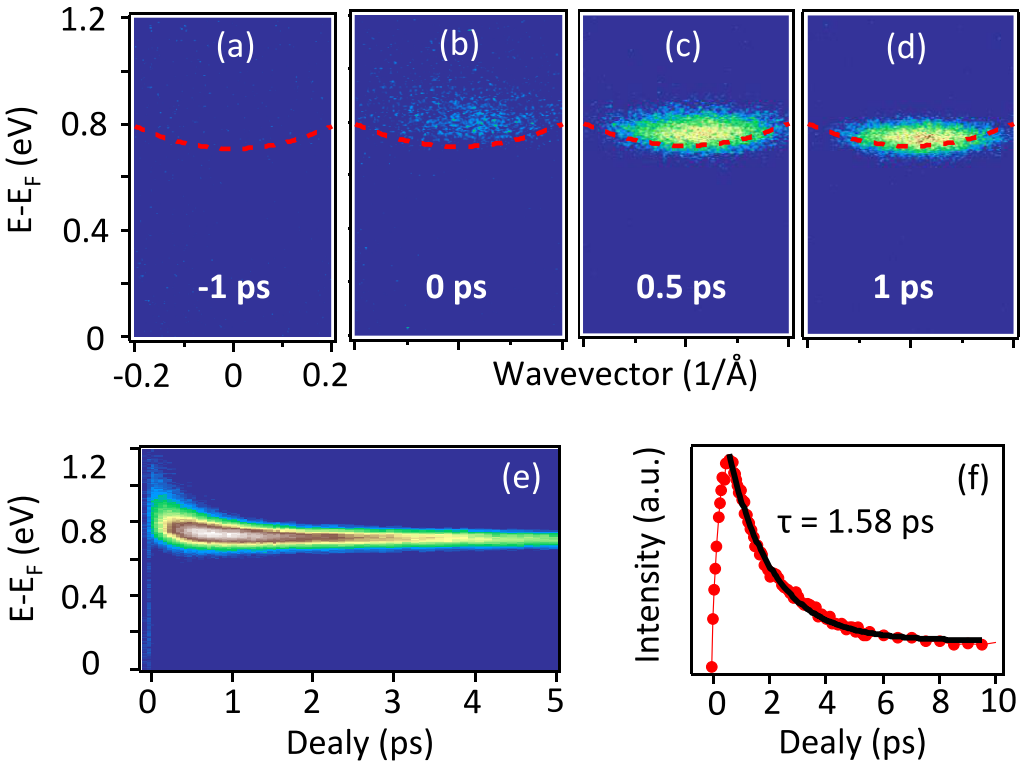

Figure 4. (a–d) Photoelectron intensity maps in GeSe acquired along the zigzag direction and plotted for different delay times. The conduction band is fitted by a parabolic function and indicated by red dashed line. (e) Dynamics of photoelectron intensity integrated in the wavevector interval $[-0.20, 0.20]$ Å^{-1}. (f) Intensity of electrons in the conduction band as a function of pump–probe delay. The black solid line is an exponential fit with decay time $\tau = 1.58$ ps.

related to the smaller matrix elements of the polar electron–phonon coupling [31]. Our observation of photoexcited states presented in this work provides useful information for further applications of InSe and GeSe in novel optical and optoelectronic devices.

Acknowledgements

We thank DIM-Oximore and the Ecole Polytechnique for funding under the project "ECO-GAN". This work was supported by the EU/FP7 under the contract Go Fast (280555) and by "Investissement d'Avenir" Labex PALM (ANR-10-LABX-0039-PALM).

References

[1] S. Hüfner, *Photoelectron Spectroscopy*, Springer, Berlin, 2003.
[2] J. Faure *et al.*, "Full characterization and optimization of a femtosecond ultraviolet laser source for time and angle-resolved photoemission on solid surfaces", *Rev. Sci. Instrum.* **83** (2012), article no. 043109.
[3] S. R. Tamalampudi *et al.*, "High performance and bendable few-layered InSe photodetectors with broad spectral response", *Nano Lett.* **14** (2014), p. 2800-2806.
[4] S. Lei *et al.*, "Evolution of the electronic band structure and efficient photo-detection in atomic layers of InSe", *ACS Nano* **8** (2014), p. 1263-1272.

[5] S. Manzeli, D. Ovchinnikov, D. Pasquier, O. V. Yazyev, A. Kis, "2D transition metal dichalcogenides", *Nat. Rev. Mater.* **2** (2017), article no. 17033.
[6] R. Roldán, A. Castellanos-Gomez, "Black phosphorus: A new bandgap tuning knob", *Nat. Photon.* **11** (2017), p. 407-409.
[7] M. J. Hamer *et al.*, "Indirect to direct gap crossover in two-dimensional InSe revealed by angle-resolved photoemission spectroscopy", *ACS Nano* **13** (2019), p. 2136-2142.
[8] N. Ubrig *et al.*, "Design of van der Waals interfaces for broad-spectrum optoelectronics", *Nat. Mater.* **19** (2020), p. 299-304.
[9] F. Xia, H. Wang, J. C. M. Hwang, A. H. C. Neto, L. Yang, "Black phosphorus and its isoelectronic materials", *Nat. Rev. Phys.* **1** (2019), p. 306-317.
[10] Z. Chen *et al.*, "Band gap renormalization, carrier multiplication, and Stark broadening in photoexcited black phosphorus", *Nano Lett.* **19** (2018), p. 488-493.
[11] Z. Zhang *et al.*, "Direct observation of band gap renormalization in layered indium selenide", *ACS Nano* **13** (2019), p. 13486-13491.
[12] T. Rohwer *et al.*, "Collapse of long-range charge order tracked by time-resolved photoemission at high momenta", *Nature* **471** (2011), p. 490-493.
[13] A. Grubišić Čabo *et al.*, "Observation of ultrafast free carrier dynamics in single layer MoS_2", *Nano Lett.* **15** (2015), p. 5883-5887.
[14] Y. Ohtsubo *et al.*, "Giant anisotropy of spin-orbit splitting at the bismuth surface", *Phys. Rev. Lett.* **109** (2012), article no. 226404.
[15] M. Caputo *et al.*, "Dynamics of out-of-equilibrium electron and hole pockets in the type-II Weyl semimetal candidate WTe_2", *Phys. Rev. B* **97** (2018), article no. 115115.
[16] G. Lantz *et al.*, "Ultrafast evolution and transient phases of a prototype out-of-equilibrium Mott–Hubbard material", *Nat. Commun.* **8** (2017), article no. 13917.
[17] C. L. Smallwood *et al.*, "Tracking Cooper pairs in a cuprate superconductor by ultrafast angle-resolved photoemission", *Science* **336** (2012), p. 1137-1139.
[18] H. Soifer *et al.*, "Band-resolved imaging of photocurrent in a topological insulator", *Phys. Rev. Lett.* **122** (2019), article no. 167401.
[19] J. Kanasaki, H. Tanimura, K. Tanimura, "Imaging energy-, momentum-, and time-resolved distributions of photoinjected hot electrons in GaAs", *Phys. Rev. Lett.* **113** (2014), article no. 237401-5.
[20] D. A. Bandurin *et al.*, "High electron mobility, quantum Hall effect and anomalous optical response in atomically thin InSe", *Nat. Nanotechnol.* **12** (2016), p. 223-227.
[21] W. Feng, W. Zheng, W. Cao, P. Hu, "Back gated multilayer InSe transistors with enhanced carrier mobilities via the suppression of carrier scattering from a dielectric interface", *Adv. Mater.* **26** (2014), p. 6587-6593.
[22] A. Gao *et al.*, "Observation of ballistic avalanche phenomena in nanoscale vertical InSe/BP heterostructures", *Nat. Nanotechnol.* **6** (2019), p. 217-222.
[23] G. Shi, E. Kioupakis, "Anisotropic spin transport and strong visible-light absorbance in few-layer SnSe and GeSe", *Nano Lett.* **15** (2015), p. 6926-6931.
[24] D.-J. Xue *et al.*, "Anisotropic photoresponse properties of single micrometer-sized GeSe nanosheet", *Adv. Mater.* **24** (2012), p. 4528-4533.
[25] H. Zhao *et al.*, "Band structure and photoelectric characterization of GeSe monolayers", *Adv. Funct. Mater.* **28** (2017), article no. 1704855-10.
[26] X. Zhou *et al.*, "Highly anisotropic GeSe nanosheets for phototransistors with ultrahigh photoresponsivity", *Adv. Sci.* **5** (2018), article no. 1800478-9.
[27] E. Doni, R. Girlanda, V. Grasso, A. Balzarotti, M. Piacentini, "Electronic properties of the III–VI layer compounds GaS, GaSe and InSe. I: Band structure", *Nuovo Cim. B* **51** (1979), p. 154-180.
[28] Y. Yang *et al.*, "In-plane optical anisotropy of low-symmetry 2D GeSe", *Adv. Opt. Mater.* **7** (2018), article no. 1801311-8.
[29] Z. Chen *et al.*, "Ultrafast electron dynamics reveal the high potential of InSe for hot-carrier optoelectronics", *Phys. Rev. B* **97** (2018), article no. 241201-5.
[30] N. Kuroda, Y. Nishina, "Anisotropies of energy-bands in GaSe and InSe", *Physica B & C* **105** (1981), p. 30-34.
[31] J. Faure *et al.*, "Direct observation of electron thermalization and electron–phonon coupling in photoexcited bismuth", *Phys. Rev. B* **88** (2013), article no. 075120.